Journal of Materials Chemistry A

Accepted Manuscript

ROYAL SOCIETY OF CHEMISTRY

www.rsc.org/materialsA

Journal Name

ARTICLE

Enhanced Photo-Electrochemical Water Oxidation on MnO_x in Buffered Organic/Inorganic Electrolytes

Received 00th January 20xx,

Fengling Zhou,[a,b] Ciaran McDonnell-Worth,[a,b] Haitao Li, [a,b] Jiaye Li,[b] Leone Spiccia*[a,b] and Douglas R. Macfarlane*[a,b]

Manganese oxide (MnO_x) materials have been widely studied as electro-catalysts for the water oxidation reaction. Although the electronic structure of MnO_2 (band gap ~2 eV) indicates it could be a promising photo-anode material for solar water splitting, so far only quite small photocurrents have been obtained from manganese oxides. Here, we show that the photo-electrochemical water oxidation performance of MnO_x films can be significantly improved by using buffered aqueous electrolytes containing amine ionic liquids. The buffered conditions to maintain a constant proton activity and the amine salt are both crucial for achieving high photocurrents. Photocurrents as high as 4.5 mA cm^{-2} were obtained at 1.0 V vs SCE (η = 540 mV) in Bi buffered n-butylammonium nitrate (BAN) electrolyte at pH9. The incident photon-to-current efficiency (IPCE) was found to be greater than 3 % at 400 nm and 4% at 370 nm. Both H_2O_2 and O_2 are produced simultaneously in this system, with the potential subsequent decomposition of the H_2O_2 to form oxygen. An acceleration of the decomposition of H_2O_2 under illumination is proposed to explain the photocurrent improvement.

1. Introduction

Photo-electrochemical (PEC) water splitting is considered to be a very promising method to store solar energy,[1] and has attracted extensive investigation.[2] One of the key factors restricting the application of water splitting as an energy technology is the lack of highly efficient, low cost and sustainable catalysts. In recent years, oxygen evolution catalysts (OECs) based on earth-abundant elements such as manganese oxides (MnO_x),[3, 4] cobalt oxides (CoO_x),[5] iron oxides (FeO_x)[6] and nickel oxides (NiO_x)[7] have been well studied due to their high catalytic activity. Manganese catalysts, which have been identified as the key element in Photosystem II, are extremely interesting.[8] We have reported that manganese molecular clusters doped into Nafion exhibit good water oxidation catalytic activity.[9] Our subsequent study revealed that the manganese cluster evolved into a material with a birnessite structure (δ-MnO_2) after applying a certain potential, indicating that the actual catalyst is a manganese oxide.[10] Different manganese oxide phases such as birnessite (δ-MnO_2),[11, 12] pyrolusite (β-MnO_2),[13] Mn_2O_3[14] and Mn_3O_4[15] have been studied as catalysts for the OER. Among these manganese oxides, MnO_2 and Mn_2O_3 have proven to offer the best catalytic performance.[14, 16] The electrodeposition process used for the preparation of the material is also important for achieving high catalytic activity. For example, the Dau group reported that the electrodeposited MnO_2 by voltage-cycling method exhibits good catalytic activity while electrodeposition at constant anodic potential produced an "inactive" material in their study.[3] By applying an ionic liquid electrolyte, MnO_x was electrodeposited at high temperature and found to exhibit higher catalytic activity than aqueous electrodeposits.[16]

In addition to the nature of the catalyst, the electrolyte is another important factor that can impact the water oxidation process and catalyst performance.[17, 18] The effects of pH have been studied, and the MnO_2 catalyst shown to exhibit higher catalytic activity at higher pH.[11] Recently, we reported a relatively low overpotential (~150 mV) water oxidation process on electrodeposited MnO_x that was achievable only in a certain family of organic salt (e.g., n-butylammonium sulphate) electrolytes.[18, 19] In this case, water can be oxidised at lower overpotential primarily to hydrogen peroxide (H_2O_2), which is stabilised by hydrogen bonding with the ammonium ion. In this respect, the process can be regarded as an n-butylammonium assisted formation of H_2O_2 electrocatalytic

[a] ARC Centre of Excellence for Electromaterials Science, Monash University, Clayton, Victoria 3800, Australia.
[b] School of Chemistry, Monash University, Clayton, Victoria 3800, Australia.
* E-mail: leone.spiccia@monash.edu, douglas.macfarlane@monash.edu.

Electronic Supplementary Information (ESI) available: The morphology of the MnO_x before and after long term testing, the thickness dependence of deposition time, the Tafel plots, the CVs in different electrolytes, the CPE measurement at different potentials, the EIS spectra in different electrolytes, The UV-Vis and Raman spectra of films, the oxygen evolution and overall faradaic efficiency measurement, the decomposition and titration of H_2O_2, and the NMR spectra of electrolyte before and after test. See DOI: 10.1039/x0xx00000x

reaction, and this process provides an alternative pathway for water splitting at lower overpotentials.[18]

Although much effort has been devoted to investigations of MnO_x, most studies have focused on the dark electro-catalytic activity.[3, 4] In fact, MnO_x could also be a promising material for photo-electrochemical water oxidation as indicated by a band structure of MnO_x that has a more positive valence band energy than the H_2O/O_2 reaction potential (**figure 1**),[20] and a band gap (Eg ≈ 2 eV, which corresponds to an absorption edge at ~600 nm) that enables light absorption in the visible part of the spectrum.[21] However, thus far, only a few studies have probed the photo-electrochemical water oxidation process on MnO_x, and these show that the MnO_x films exhibit quite poor photo-activity for water oxidation.[22, 23] Well-defined, dispersed nanoparticles MnO_x formed by incorporating Nafion showed significant photo-activities, with photocurrents similar to the dark currents measured at overpotentials of 150-550 mV.[24] However, the low loading of MnO_x in these photo-anodes meant that the photocurrents were relatively small (<0.1 mA cm^{-2}). In general, the photo-activity on MnO_x is still quite low compared to other typical photo-electrochemical water oxidation catalysts, such as Fe_2O_3[6] and $BiVO_4$,[25] and the investigation of MnO_x as photoanode is still at a very early stage.

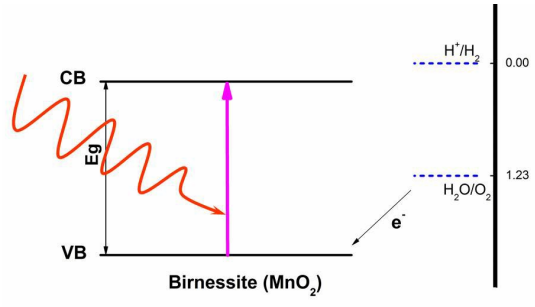

Figure 1. Schematic band structures of manganese oxides (Birnessite) with reference to the H_2O_2/O_2 reaction.

The light intensity has been proven to affect the photocurrent generated on photoelectrodes in previous studies,[26-28, 29] and an illumination of AM1.5 100 mW cm^{-2} is usually applied in the research.[6, 25, 30-32] On the other hand, in practical applications, the solar light intensity can be easily magnified using solar concentrators. This approach has been used in concentrating photovoltaic (PV) systems to focus sunlight onto a small PV chip, producing highly efficiency.[33] This could potentially reduce the overall cost of solar systems in general since the solar collector is typically less expensive than the equivalent area of solar cells. Similarly, in solar water splitting, the use of a solar concentrator has the exciting potential to generate higher efficiencies and result in lower costs. Thus, it is important for photoelectrodes to maintain high efficiency under strong illumination. Here, we study the effect of concentrated solar illumination on MnO_x water oxidation electrodes. For MnO_x to become an efficient photo-electrode, further work is needed to improve the photo-electrochemical performance, by optimising both the electrolyte and also the crystalline structure and morphology[6] to enhance the photon-absorption efficiency and the photo-generated carrier transport rate. We focus on the role of the electrolyte in the photo-water oxidation process and demonstrate that the photo-electrochemical oxidation of water is enhanced by the introduction of a buffered alkylammonium ionic liquid electrolyte. The process is shown to produce both oxygen and hydrogen peroxide at low overpotentials. The effects of substrate, film thickness and illumination direction are studied and optimised and, thereby, photocurrents as high as ~4.5 mA cm^2 (η = 540 mV) have been achieved on the MnO_x film.

2. Experimental Section

Materials

All reagents were purchased from commercial supplies and used as received unless stated otherwise. Deionised water was used for all experiments. Ethylammonium nitrate (EAN) or n-butylammonium nitrate (BAN) were prepared by neutralising the ethylamine (EA) or butylamine (BA) with dilute nitric acid (HNO_3), followed by removal of the water under reduced pressure by rotary evaporation at 50 °C for 2 hours.

Film deposition

The manganese oxide (MnO_x) films were prepared by electrodeposition in a three-electrode electrochemical system from an ionic liquid electrolyte, as described in greater detail elsewhere.[16, 18] The deposition electrolyte (2 ml in volume) contained 10 mM $Mn(CH_3COO)_2$ in a 1:9 water to EAN mixture. It was acidified slightly by adding 10 µl of 2.0 M HNO_3 to give a 10 mM excess of acid. The MnO_x film prepared using this electrolyte was denoted as sample A1 in our previous report.[16] Fluorine-doped tin oxide (FTO) conducting glass or a gold (Au) sheet with an active electrode area of 0.5 cm x 0.5 cm was used as substrate for film deposition. The MnO_x film was electrodeposited at 120 °C by applying a constant current density of 200 µA cm^{-2}. Following exploratory studies to determine the optimum deposition time, a time of 30 min was generally used to prepare the film, unless otherwise specified. After deposition, the films were rinsed thoroughly with distilled water.

Photo-electrochemical measurements

The photo-electrochemical performance was measured in a three-electrode system on the VMP2 potentiostat system. Generally, the MnO_x films and Ti foil were used as the working and counter electrodes, respectively with Ag/AgCl or saturated calomel electrode (SCE) reference electrode. The potential of the Ag/AgCl reference electrode was -60 mV vs SCE.

A 1.0 M n-butylammonium nitrate (BAN) solution of pH9 or pH10 was prepared by adding 1.2 mol % and 11.2 mol % of extra n-butylamine (BA) into the BAN solution, respectively. The 0.20 M of borate buffer (Bi) at pH9 was prepared by adding boric acid solution (H_3BO_3) into a 0.05 M sodium borate solution ($Na_2B_4O_7{\cdot}10H_2O$), whereas the pH10 buffer was prepared by adding sodium hydroxide solution into the sodium borate solution. The mixed electrolytes at pH9 or pH10 were obtained by mixing the (pH9/pH10) BAN solutions with Bi buffer (pH9/ pH10), and then slightly adjusting the pH of the mixture to 9 or 10 by adding either H_3BO_3 or BA. Typically, 10 ml of electrolyte was used for the photo-electrochemical measurements.

Linear scan voltammetry (LSV) and controlled potential electrolysis (CPE) were used to characterize the catalytic performance with respect to water oxidation. The LSVs were usually carried out by sweeping from 0.3 V to 1.2 V vs SCE at a scan rate of 5 mV s^{-1}. The CPE was conducted by applying a constant potential of 0.4 - 1.2 V vs SCE at room temperature. In the LSV test, the dark and light LSV were measured in the same electrolyte, with the dark LSV tested first. In all other measurement, fresh electrolytes were used.

Except for the IPCE measurements, all photo-electrochemical measurements were made using a 300 W Xe lamp as the light source. The intensity of the light was controlled by varying the distance between the light source and sample. In typical measurements, the distance was kept at 2 cm, where the light intensity equals about 9 suns (calibrated with Thorlabs optical power and energy meter PM110D equipped with S310C thermal sensor), and most of the photo-electrochemical experiments were done at this light intensity using back-side illumination unless otherwise specified.

Incident Photon to Current Efficiency (IPCE) measurements were made using a 150 W Oriel solar simulator, equipped with an AM1.5G filter, as the light source. A series of filters were used to cut the light to monochromatic light from 370 nm to 570 nm having bandwidths of 20 nm. The total light intensity for the IPCE measurement was about 3 suns, hence for each 20 nm band the intensity is about 1~6% sun (1~6 mW cm^{-2}) depending on the transparency of filters. An electrolyte containing 0.20 M Bi buffer and 1.0 M BAN at pH9 was used to measure the IPCE, and a constant potential of 1.0 V vs SCE was applied during the test. The IPCE was calculated as follows:

$$\text{IPCE }\% = \frac{electrons/sec}{photons/sec} = \frac{I(mA)\times 1240}{P(mW)\times\lambda(nm)}\times 100$$

where *I(mA)* indicates the photocurrent (mA cm^{-2}), *P(mW)* indicates the input light intensity (mW cm^{-2}) and λ represents the wavelength of monochromatic light. The number of 1240 is the value of $hc/(e \times 10^{-9})$, with *h*, *c* and *e* are Planck's constant, speed of light and electron charge, respectively.

Electrochemical impedance spectroscopy (EIS) measurements were carried out from 0.4 to 1.0 V vs SCE in dark and under illumination. The EIS measurement frequencies were varied from 200 kHz to 0.1 Hz, using an amplitude of 10 mV. The spectra were fitted to an equivalent circuit model using the ZView software.

Film characterization

Film thickness was measured by using a Dektak 150 surface profiler. The absorption spectrum of the film is measured on a Jasco V-670 UV-Vis spectrophotometer. The morphology of the film was analysed using the scanning electron microscopy (SEM) secondary image, which was conducted at 30 kV with a working distance of 6 mm on a JEOL 7001F FEG SEM. Raman spectra were recorded with a Renishaw inVia Raman microscope using a 514 nm incident laser.

NMR Spectroscopy

The electrolyte for NMR spectral measurement was prepared by using D_2O as the solvent, and the electrolyte contained 0.10 M Bi and 1.0 M BAN, at pH9. Proton NMR measurements were conducted on a Bruker AvanceIII 400 spectrometer. NMR signals were collected on the electrolytes before and after photo-electrochemical testing under ~9 suns illumination.

Oxygen and hydrogen peroxide measurements

Oxygen measurements were conducted in a home-built gas-sealed three-electrode cell. A 6 ml solution of 0.10 M Bi buffer containing 1.0 M BAN at pH9 was added into the cell, leaving a head-space volume of 26 ml. The oxygen in the head space was measured using a fluorescence probe, as detailed elsewhere.[16] The fluorescence probe is very sensitive to light, and the gas expansion under illumination causes a pressure change. Thus, the oxygen measurement under illumination condition was conducted by measuring the oxygen level in the head space of the cell before and after PEC experiment.

The amount of hydrogen peroxide was measured by titration in a UV-Vis cell, using potassium permanganate as oxidant, as detailed in the literature.[18] Typically, 0.25 ml of the electrolyte was added into 0.25 ml of 1M H_2SO_4, and a solution of 0.00755 M potassium permanganate was used for the titration. UV-Vis absorption spectra were recorded at room temperature on a Cary 300 Bio UV-Visible spectrophotometer and the permanganate concentration was determined from the absorbance at 565 nm.[18] A control experiment was conducted and the results (figure S1) show that in this titration no amine was oxidized by the permanganate.

Hydrogen production is observed on the counter electrode with formation of bubbles during the PEC process. The GC measurement of the collected gas confirms the production of hydrogen.

3. Results and Discussion

3.1 Photo-electrochemical Performance

The MnO_x film deposited from acidic ionic liquid (A1) for 10 mins at 120 ^{o}C on FTO substrate served at the photo-anode for the photo-electrochemical measurements. The obtained film has a nano-sized fibrous structure (figure S2a) with a thickness around 900 nm. XRD has been conducted in our previous study,[16] and no peak

attributable to MnO_x was observed. Extra characterization of the material carried out in that work by EXAFS and EDS indicates that this film corresponds to the typical birnessite phase, as detailed in our previous report.[16]

The linear scan voltammetry (LSV) was measured in several electrolytes in the dark and under illumination to evaluate the photo-electrochemical performance of the MnO_x film. Figure 2 shows the LSVs of the MnO_x in three electrolytes at pH9: (i) 1.0 M n-butylammonium nitrate (BAN); (ii) 0.20 M borate (Bi) buffer; and (iii) a mixture of 0.10 M Bi buffer with 0.50 M BAN. The LSV measured in the Bi buffer (black dashed line) exhibits a clear onset of dark current at about 0.9 V vs SCE, while it appears at around 0.6 V vs SCE in the BAN solution (blue dashed line). For the BAN/buffer mixture (red dashed line), which was obtained by mixing the BAN solution at pH9 and Bi buffer at pH9 and slightly adjusting the pH to 9, the onset of dark current occurs at 0.6 V vs SCE, which is same as that in the BAN solution (figure 2, blue dashed line).

Under illumination (solid lines), the film exhibits photo-activity in all the three electrolytes, shown as solid lines in figure 2. There is a decrease in the onset potential and a current density increase under light. Under illumination, the Bi buffer (black lines) exhibits either little or no photocurrent below 0.8 V. The highest photocurrent in the measured region in the Bi buffer is ~0.5 mA cm^{-2} at 1.2 V. The most important observation is that the photocurrent in the mixture (red line) is much higher than that of either of the two other electrolytes (black lines for Bi and blue for 1.0 M BAN). The photocurrent increases with the applied potential below 1.0 V, and reaches a plateau at higher potentials, as is normally observed with photo-electrodes.[6, 34]

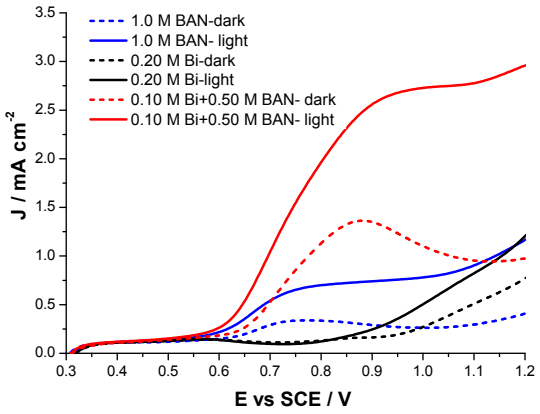

Figure 2. LSVs of MnO_x film measured in different electrolyte at pH9 in dark and under ~9 suns illumination from back side of FTO.

The thickness of the films has been proven to be an important factor in the photo-activity of photo-electro active materials.[35] In the preliminary experiment shown in figure 2 the MnO_x film was obtained by a 10 minute deposition. The films thickness can be tuned by varying this deposition time, i.e., the longer the deposition time, the thicker the films.[22] Figure S3 shows the thickness of MnO_x films obtained from different deposition time, exhibiting a linear relationship. LSVs of MnO_x films with different thickness were measured in the dark and under light as shown in figures S4 and 3. It can be seen that the film deposited for 5 minute has the highest activity in dark, whereas the thicker film shows a slightly decreased dark current (figure S4). This could be due to lower carrier collection efficiency in the thicker film.[22] On the other hand, due to more material in the thicker film, more light can be absorbed, and this results in higher photocurrents, as shown in figure 3. Whereas, for the very thick films, both the resistance within film increases and also the pathway for charge carrier migration to the semiconductor surface increases which increases the recombination rate and limits the photocurrent.[36] In this study, the film with thickness of 4 µm from a 30 min deposition exhibited the highest photocurrent while the photocurrent decreased at a longer deposition time (45 min). Therefore, unless otherwise stated, the MnO_x films prepared using a 30 min deposition time were used in the measurements and characterization studies that follow.

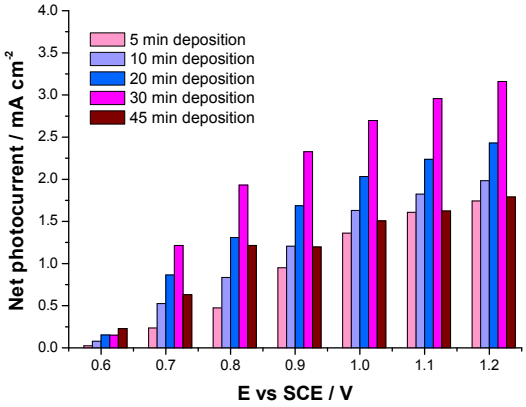

Figure 3. Net photo-current density of MnO_x films with different deposition times, measured in 0.10 M Bi+0.50 M BAN electrolyte at pH9.

The influence of the substrates was also considered and it was found that the film deposited on Au exhibits a slightly higher activity than that on FTO glass under illumination (figure S5). This might be due to the better conductivity of the Au substrate, which decreases the system resistance and allows the electrode to carry higher currents; the reflectance of the Au electrode may also increase the optical path length in the semiconductor and results in better utilization of the light.[37, 38]

The effect of the side of illumination on the photo-electrochemical performance on MnO_x was investigated on the FTO glass electrodes. Figure S6 shows the CV of MnO_x in dark and under different illumination conditions. The CV plot exhibits pre-peaks (0.59 V in dark and 0.55 V under illumination) before water oxidation starts. These peaks has been related to the changes of the surface oxidation states.[39]

It can be seen that the photocurrents measured for back-side (substrate side) and front-side (electrolyte side) illumination were very similar. The illumination direction can have a significant influence on the performance of nanostructured semiconductor films. Normally, such films exhibit lower photocurrents under front-side than under back-side illumination, as has been observed on Fe_2O_3[40] and $BiVO_4$.[31] This is because for front-side illumination the photo-generated charge carriers need to penetrate the film before they are collected by the conducting substrate, whereas for back-side illumination they can be more directly and efficiently collected by the substrate, leading to higher photocurrents.[31, 40] In contrast, Sasaki and co-workers[23] reported higher IPCEs for front-side illumination than that for back-side illumination on MnO_2, and proposed that only the topmost layer could generate photocurrent in their films.

The negligible difference between front-side and back-side illumination in this study indicates that the mobility of the photo-generated electrons in the MnO_x film is not a strongly limiting factor in photocurrent generation. This is consistent with the film thickness study above that showed that a reasonably thick film generates the highest photocurrent.

To further understand the intrinsic activity of the film in different electrolytes, a Tafel-analysis was performed at pH9 under dark and illumination conditions, as shown in figure 4. The 30 min deposited film in the Bi buffer exhibits a large Tafel slope (cyan line, 153 mV/dec), while notably in the BAN/Bi buffer mixture (black line), the Tafel slope is much smaller (~ 90 mV/dec). Furthermore, the Tafel slopes for the 30 mins deposited film, measured in the mixture electrolyte in the dark (figure 4, black line, 96 mV/dec) and under illumination (figure 4, red line, 91 mV/dec) are the same; however, the Tafel region shifts to lower overpotentials under illumination due to the photo-enhanced activity. For the BAN electrolytes, the Tafel slope is 92 mV/dec (figure 4, blue line), which is similar to the value in the mixture electrolyte. The significant difference of the Tafel slopes measured in the different electrolytes indicates that the water oxidation mechanism may be different in the presence and absence of BAN.

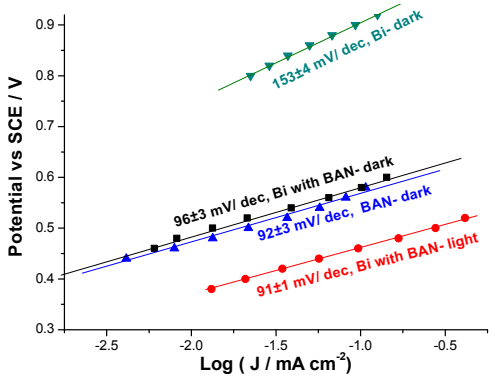

Figure 4. Tafel plots of MnO_x film deposited for 30 mins, measured in different electrolytes at pH9 in dark and under light.

Further investigation of the effect of film thickness on the Tafel slope is shown in figure S7. Compared with the 30 mins deposited films, a 5 mins deposited film exhibits lower Tafel slopes. The larger Tafel slope for the thicker film is expected due to the decreasing electro-activity in the thicker films as shown in the dark current plot (figure S4). The change of slope, for example in the mixture from 93 mV/dec to 59 mV/dec (figure S7b), indicates that the catalysis mechanism is different. A similar effect that thinner films exhibit lower Tafel slopes was also observed on a Pt–Pd–rGO electrode used for the hydrogen evolution reaction.[41] This might be due to the surface states varying in the thicker films, and lowering the electro-catalytic activity. Increasing resistance in the thicker film could also contribute to a larger Tafel slope.

The influence of the BAN and Bi concentration in the mixed electrolyte on the dark current and photocurrent was also investigated and the data are shown in figures S8 and 5a. In the dark, the current could be improved by increasing the Bi concentration while variation of the BAN concentration had no significant effect (see figure S8). Under illumination, an increase in the BAN concentration in the mixture improves the photocurrent (figure 5a). Variation of the Bi buffer concentration in the mixture also affects the photocurrent (figure 5a); the 0.1 M Bi with 1.0 M BAN electrolyte results in a smaller photocurrent density (3 mA cm^{-2} at 1.0 V) than 0.20 M Bi with 1.0 M BAN (4.5 mA cm^{-2} at 1.0 V, η = 540 mV). The highest photocurrent of ~4.5 mA cm^{-2}, measured in 0.20 M Bi with 1.0 M BAN, is quite remarkable when it is compared to a value of <0.1 mA cm^{-2} reported previously for MnO_2 studied under more intense illumination conditions (~10 suns)[22] than used herein (~9 suns).

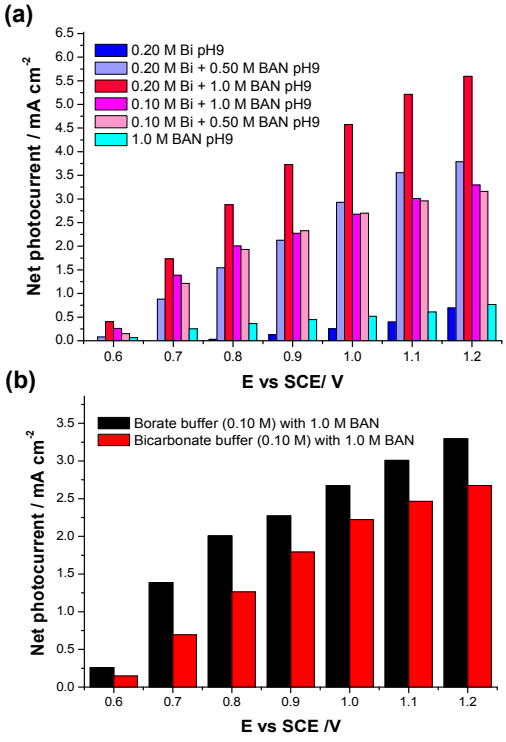

Figure 5. (a) Photocurrent density of MnO_x films measured in different electrolytes at pH9. (b) MnO_x photocurrents measured in Bi buffered BAN electrolyte (black), and bicarbonate buffered BAN electrolyte (red) at pH9. The net photocurrent is obtained from LSVs plots by subtracting the dark current (figure S8) from the total current.

In order to investigate whether the increase in photocurrent for the electrolyte mixture is specifically due to the presence of the borate buffer, a bicarbonate buffer mixed with the BAN solution was also studied. Replacement of the Bi buffer with the bicarbonate buffer results in a similar photocurrent, as shown in figure 5b. However, if the Bi buffer is replaced with $NaNO_3$, the LSV behaviour is similar to that measured with the BAN electrolyte solution (see figure S9); i.e., only small dark and photocurrents were observed. This indicates that the improved photocurrent is probably due to the use of buffered electrolytes, rather than any particular buffer anions/cations.

Ethylammonium nitrate (EAN) is another common amine based ionic liquid with a similar structure to BAN. Replacing BAN in the electrolyte mixture with EAN reveals that both electrolytes result in high photocurrent densities (figure S10). Thus, the high photocurrents are not limited to the BA-based electrolyte, indicating that other amine cations can indeed be used. The slightly lower photocurrent for the EAN/Bi electrolyte mixture may be due to the slightly smaller size of the cation used or the pKa difference (BA: 10:59;[42] EA: 10.70[43]); this is under further investigation.

The borate in the mixture could just play the role of a buffer for the amine ions based electrolytes. As the pKa of butylamine is 10.59,[42] a BAN electrolyte with a higher pH (~10) could be considered to be a self-buffered electrolyte (n_{BA} : n_{BAN}= 0.11:1 at pH=10). In order to find whether the borate based inorganic electrolyte is essential for obtaining high photocurrent, further testing was conducted in BAN electrolytes with and without Bi, and the results are shown in figure 6. In order to better compare the activity at different pHs, the applied potentials have been converted to overpotentials ($\eta = E - E_0$). The dark current density in the BAN/Bi mixture at pH10 (2.7 mA cm^{-2} at η = 0.5 V) is much higher than that in the electrolytes with the same composition at pH 9 (1.1 mA cm^{-2} at η = 0.5 V). This is probably due to the expected increase in activity of MnO_x at higher pH.[11] Under illumination, the photocurrent measured for the BAN electrolyte at pH10 (2.9 mA cm^{-2} η = 0.5 V), is more than three times than that at pH9 (0.5 mA cm^{-2} at η = 0.5 V)). Similarly, the photocurrent in the pH10 BAN/Bi electrolyte mixture is 3.5 mA cm^{-2}, which is 50% higher than that at pH9 (2.5 mA cm^{-2}). Thus, increasing the pH clearly results in a effective increase photocurrent in the BAN, and it indicates that the buffer conditions (by self-buffering or adding inorganic buffer electrolyte) in the presence of the BAN is very important for and affords substantial increases in high photo-activity.

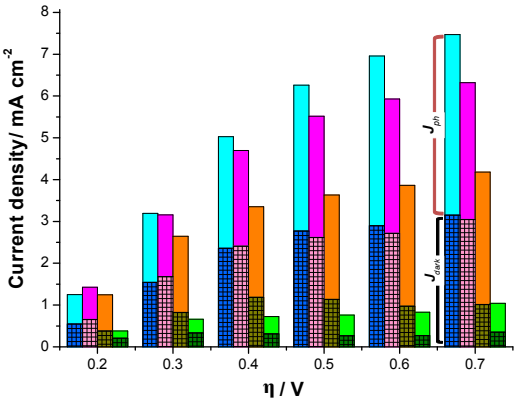

Figure 6. Dark current (filled bar with grid) and photocurrents (filled bar without grid) on MnO_x measured at different potentials obtained from LSV plots, in 1.0 M BAN + 0.10 M Bi at pH10 (blue), 1.0 M BAN at pH10 (pink), 1.0 M BAN + 0.10 M Bi at pH9 (orange), 1.0 M BAN at pH9 (green).

CPE measurements were conducted at different potentials on the MnO_x deposited on FTO with back side illlumination, as shown in figures 7 and S11. The steady-state photocurrents determined by this means are independent of the scan rate and measurement history.[34] Figure 7 clearly shows that illumination generates a reproducible photocurrent. The steady-state photocurrent when a pH9 buffer/BAN electrolyte is used is ~3 mA cm^{-2} is much higher than for the Bi buffer (~0.2 mA cm^{-2}) and BAN solution (~ 0.3 mA cm^{-2}), as expected from the LSV results in figure 2.

The decay of the photocurrent back to zero from the time the light is switched off takes as long as ~150 s for the BAN/buffer mixture (see last cycle of the blue line in figure 7). This behaviour is not normal for semicondutors, but has also been observed for some other photoelectrodes.[44] This slow photocurrent decay may originate from: 1) the heating effect of the intense light; and/or 2) slow charge carrier diffusion in the MnO_x film or electrolyte. The temperature of the electrolytes was measured before and after each test (overall illumination for 120 s as shown in figure 7) and the observed variation is only ~2 ^oC, indicating that heating effects may not be an important factor. This conclusion is strongly supported by fact that a similar slow current decay is observed when the BAN electrolyte without the Bi buffer is used (red trace in figure 7), and that such current-decay behaviour is not observed for the measurements applying only the Bi buffer (see sharp rise on switching in the black trace in figure 7). Additional CPE measurements, conducted at different potentials (see figure S11a-c) provide further evidence against heating effects being a factor. At low potentials (0.4 V in figure S11a and 0.6 V in figure S11b), the photocurrent increases and decreases instantly on switching the light on and off. It is at higher potentials in the presence of BAN, where the currents

are higher (1.0 V and 1.2 V in figures S11c and 7), that switching results in longer photocurrent transients. This indicates that a slow build up and decay of the steady state population of photo-excited electrons and holes may be the origin of these effects; this behaviour will be further discussed later. A longer term experiment (more than 1 hr illumination of the MnO_x film) does not show an obvious decrease of the photocurrent with time (figure S11d) and, moreover, the morphology and the Raman spectra of the film does not change significantly after long term testing (figure S2). Thus, the MnO_x photo-catalyst is stable during prolonged photo-electrochemical water oxidation.

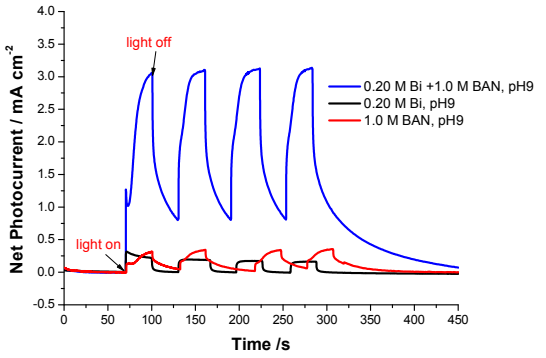

Figure 7. CPE measured on MnO_x films in different electrolytes at pH9 under chopped illumination from the back side. Arrows show the turning of the light on and off. The photocurrent was obtained by subtracting the dark current from the overall current. Conditions of test: 1.0 V (vs SCE) under ~9 suns light intensity.

Electrochemical impedance spectroscopy (EIS) was used to study the charge transfer during water oxidation as shown in figures S12. The semicircle in the high frequency range for a particular electrolyte shows no change in the position and the radius by varying the applied potential, but decreases a little on illumination (illuminated and dark EIS are compared in figure S12 a, b, c). The fitted parameters (table S1) show that the resistance R_1, usually related to the resistance of the film and electrolyte as well as contacts in the circuit,[38, 45] is smaller in the mixture and BAN solution than that in Bi buffer. This is likely due to the better conductivity when a higher concentration electrolyte is used. At low frequencies, another semicircle appears and its radius under illumination is smaller than in the dark at higher potentials. This semicircle varies with applied potential (figure S12a, b, c) and is understood to be associated with the water oxidation reaction.[38, 46] A comparison of the Nyquist plots at 1.0 V, see figure S12d, shows that the radius of the semicircle at low frequencies is much smaller (under illumination) in the Bi buffer and BAN/Bi mixture than in BAN. The fitted parameters indicate a higher charge transfer resistance (Rp) for the water oxidation reaction in the BAN electrolyte, as expected from the LSV plot at this potential (figure 2). The BAN/Bi mixture exhibits the smallest Rp indicating a significant decrease in the water oxidation charge transfer resistance, as expected from the higher photocurrents shown in figures 2 and 3.

Figure S12e shows the impedance spectroscopy of the MnO_x films at pH10 at 0.8 V. Two semicircles can be observed in the impedance spectra for both the BAN and mixture electrolytes. This indicates that at pH10, where the BAN solution is self-buffered, there is a similar charge transfer resistance to that for the mixture. This is again concordant with the similar photocurrents shown in figure 6.

3.2 Optical Properties and IPCE Measurement

UV-Vis spectrophotometry was used to investigate the optical properties of the MnO_x films, as shown in figure S13 and Figure 8 (blue line). The film exhibits absorption up to 650 nm. The Tauc plot of the variation of $(\alpha h\nu)^{1/2}$ and $(\alpha h\nu)^2$ with photon energy, inset to figure 8, shows an energy gap for the indirect (2.25 eV) and direct transitions (2.7 eV) in MnO_x films, which are close to literature reports for birnessite MnO_2 films (2.1 eV and 2.7 eV, respectively).[22] Calculations of vacancy-free MnO_2 shows that it is an intrinsic indirect band gap material, while the existence of Ruetschi defects (Mn(IV)) can introduce a direct excitation.[47] Both the indirect band gap energy and direct band gap energy can be observed in MnO_x, as shown in this research and in the literature.[22] The existence of the indirect band gap is considered to cause a decrease in the recombination rate of the photo-excited electron-hole pairs, which can improve the photo-activity (for example, anatase TiO_2 which has an indirect band gap usually exhibits a higher photo-activity than rutile TiO_2 which has only a direct band gap).[48]

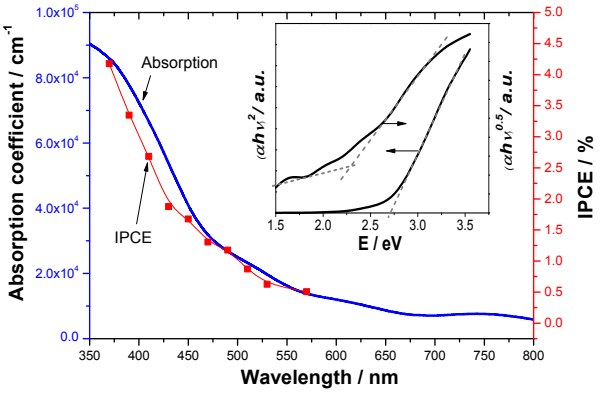

Figure 8. UV-Vis spectra and IPCE results. (Blue line) Absorption coefficient was calculated from the transmittance spectra of the thinnest MnO_x film (figure S13). Inset shows the variation of $(\alpha h\nu)^{1/2}$ and $(\alpha h\nu)^2$ with photon energy for the MnO_x film; the horizontal intercept represents the energy gap of the indirect and direct transitions respectively. (Red dotted line) IPCE results for the MnO_x film on FTO in 0.20 M Bi buffer +1.0 M BAN electrolyte (pH9). The test was conducted whilst applying a constant potential of 1.0 V vs SCE under monochromatic light (1-6 mW cm^{-2}).

The photocurrents generated under monochromatic light (20 nm bandwidth) were measured at a relatively high potential (1.0 V vs SCE in 0.20 M Bi with 1.0 M BAN electrolyte at pH9) to ensure the accuracy of the measurements. The incident photon to current efficiency (IPCE) is calculated as detailed in the experimental section, and is plotted as a function of the excitation wavelength in figure 8 (red dotted line). The IPCE follows the absorption spectrum, increasing significantly below 450 nm. The highest IPCE of ~4% was achieved at the lowest wavelength measured (370 nm) and was above 3% at 400 nm. Thus, the MnO_x film more effectively converts incident photons to current at the shorter wavelengths. Compared to the absorption spectrum (blue line in figure 8), the IPCE spectrum shifts slightly to shorter wavelengths. This phenomenon has been observed previously in MnO_2[22] and Fe_2O_3[40, 49] and may be due to a predominance of indirect band-gap transitions under illumination at longer wavelengths, which are of lower energy and hence lower the efficiency of photocurrent generation at these wavelengths.[22, 49]

The IPCE efficiencies determined in this study are much higher than previous reported values for MnO_x, which well below 1%.[22, 23] The remarkable improvement in IPCE presented herein could be partly due to the optimisation of the MnO_x film with respect to thickness, and more importantly to the significant enhancement in photo-electrochemical activity afforded by using buffered amine-based electrolytes.

In this study, the photo-electrochemical performance was mostly recorded under a high light intensity (~9 suns), which is much higher than that normally used in similar studies (~1 sun).[6, 30] In order to study the influence of light intensity, the steady-state photocurrents at different intensities were measured, as shown in figure 9. The photocurrent increases linearly with the light intensity and, over the intensity range studied, does not show any signs of reaching a saturation limit of the sort seen in other materials such as CdS.[26] The linear relationship reveals that charge is transferred rapidly at the interfaces,[29] otherwise recombination would become more dominant as it is dependent on the square root of intensity.[29] The linear dependence observed here indicates that the photocurrents generated by the MnO_x films can potentially be further enhanced by working at even higher light intensities.

The photocurrent (J_{ph}) at 1 sun can also be estimated by integrating the IPCE spectra (Figure 8) from 370-570 nm using a method detailed elsewhere;[50] and yields a value of 0.2 mA cm^{-2}. Under 1 sun illumination, the measured photocurrent at 1.0 V was 0.4 ± 0.15 mA cm^{-2} (Figure 9). The slightly underestimation in J_{ph} from the IPCE data partly arises from the fact that the measurement does not cover the whole solar spectrum.

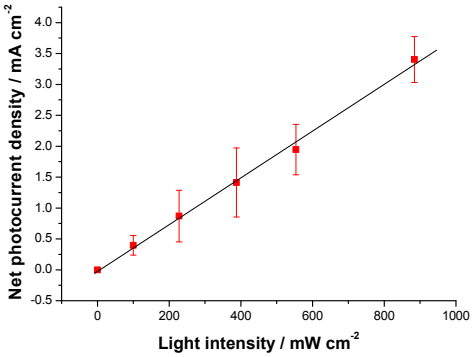

Figure 9. The influence of light intensity on the steady state photo-current density of MnO_x films tested in 0.20 M Bi buffer + 1.0 M BAN electrolyte (pH9) at 1.0 V vs SCE. Each data point is the mean of measurements on three different samples (error bar = s.e.m.)

3.3 Oxygen and Hydrogen Peroxide Production

We previously reported that the n-butylamine (BA) cation is stable without any decomposition or oxidation observed during water oxidation in dark conditions.[18] In order to check whether BA decomposes under light, NMR spectra of the electrolyte were recorded before and after water oxidation under light. The spectra show no evidence of decomposition products being formed (figure S14) confirming that the increase in the current density under light does not result from decomposition of the electrolyte.

Our previous work has shown that H_2O_2 is a significant product in the buffered amine electrolytes.[18, 19] The controlled experiment with commercial H_2O_2 shows no effect on the onset of the LSV plots of MnO_x in the examined electrolytes (figure S15). To determine the H_2O_2 production efficiency, a constant potential of 1.0 V vs Ag/AgCl was applied for 2 hours on the MnO_x, both in the BAN electrolyte and the mixture (and also in Bi as a control experiment), with and without illumination. The amount of H_2O_2 was determined by titration in a UV-Vis cell, as detailed in the experimental section and literature.[18] The H_2O_2 production efficiency, calculated by using Faraday's law and assuming a 2-electron water oxidation process, is shown in table 1. In the dark, the 1.0 M BAN produces 3.1 µmol H_2O_2 in 2 hours, equivalent to a 70% Faradaic efficiency, and the buffer/BAN mixture produces 3.4 µmol H_2O_2, which indicates a 63% Faradaic efficiency. The lower than 100% H_2O_2 production efficiency is due to the further oxidation or decomposition of H_2O_2 to O_2, or the competing process of water oxidation to oxygen.[18] In contrast, in the Bi buffer, only O_2 is produced and no H_2O_2 was found (table 1), as reported previously under the similar conditions.[13] The plot in Figure S16 shows a combined Faradaic efficiency of 94±7% for the water oxidation process (H_2O/H_2O_2 + H_2O/O_2) in the dark, confirming that, within experimental error, all the current is used for water oxidation.

Table 1. H_2O_2 production and Faradaic efficiency (measured at 1.0 V vs Ag/AgCl)

	H_2O_2 production in 2 hours (μmol) [a]	H_2O_2 production efficiency (%) [b]
1.0 M BAN, pH9 - dark	3.1± 0.1	70±3
1.0 M BAN, pH9 - light	2.2±0.1	27±1
0.10 M Bi buffer + 1.0 M BAN, pH9 - dark	3.4±0.2	63±3
0.10 M Bi buffer + 1.0 M BAN, pH9 - light	3.3±0.1	24±1
0.20 M Bi, pH9 – dark [c]	-0.06±0.15	-
0.20 M Bi, pH9 – light [c]	-0.06±0.22	-

[a] amount of H_2O_2, measured from by titration in a UV-Vis cell as detailed in the experimental section and literature.[18] [b] H_2O_2 production efficiency calculated as follows: (amount of measured H_2O_2) /(the calculated amount of H_2O_2 by using Faraday's law and assuming a 2-electron water oxidation process) x100. [c] the measured amount of H_2O_2 in Bi in dark and under illumination is just errors, indicating no H_2O_2 produced in Bi.

Under illumination, the amount of H_2O_2 produced is similar to that in dark in both electrolytes, but the corresponding H_2O_2 production efficiency drops significantly (because the overall current is increased) from 70% to 27% and from 63% to 24%, respectively. Furthermore, the combined Faraday efficiency for O_2 (75±2%) and H_2O_2 (27±2%) production, determined from the same experiment under illumination (Table S2), was 100% (102±4%). This implies that either (i) the photocurrent increase is principally the result of a direct water to oxygen process[51] or (ii) the illumination is accelerating the H_2O_2 decomposition to O_2 on or near the electrode.[52] The accelerating effect of illumination on the decomposition of H_2O_2 on MnO_2 particles is confirmed by the results shown in Figure S17. This is in accordance with the previous results[52] where illumination was found to result in rapid decomposition of H_2O_2.

3.4 Mechanistic Considerations

Much fundamental work has been carried out on the mechanism of water oxidation by electrolysis. Under alkaline conditions, the first step in the water oxidation reaction on the non-noble metal oxides, such as Ni, Mn, Co and $SrFeO_3$ was proposed to involve a one electron process to form a surface (Σ) bound hydroxyl species:[53, 54]

$\Sigma + H_2O \rightarrow \Sigma\text{-}OH + H^+ + e^-$ (equation 1)

Slow oxidative cleavage of the Σ-OH bond then forms a peroxide species:[53, 55]

$\Sigma\text{–}OH + OH^- \rightarrow \Sigma + H_2O_2 + e^-$ (equation 2)

$2H_2O_2 \rightarrow O_2 + 2H_2O$ (equation 3)

Once formed, the peroxide (H_2O_2) will disproportionate into O_2 (equation 3) or be further oxidised to O_2.[53] As summarised in the schematic diagram in figure 10, In the presence of the ammonium cation/amine mixture, the H_2O_2 is solvated and its production thereby enhanced.[18] However, irradiation is known to cause a significant increase in the rate of H_2O_2 decomposition[52] in solution. The increased photocurrent under illumination observed in the present work could therefore be the result of the decomposition of H_2O_2 to dioxygen, thus decreasing the steady state H_2O_2 concentration and accelerating the water oxidation reaction.

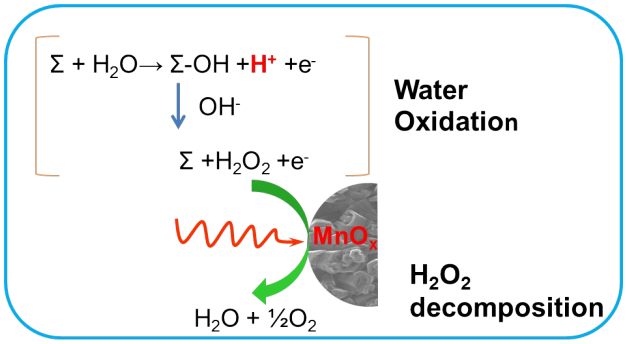

Figure 10: Schematic diagram showing the water oxidation reaction and H_2O_2 decomposition on MnO_x.

The CPE measurement with the slow increase at light on and slow decay at light off (figure 6, S11) clearly illustrates the influence of illumination on the photocurrent in the presence of BAN. The detailed photocurrent under CPE measurement shows it is composed of two parts: an initial fast response followed by a slow response as shown in figure 11. The fast photocurrent response can be observed instantly with light on and light off, followed by another, slower photocurrent response. Normally, the photocurrent resulting from the photo-generated electron-hole is determined by the mobility and separation efficiency of electron-hole pairs, and the response time varies but does not exceeds several seconds in normal cases.[56] Thus, the fast photocurrent response in figure S11 is attributed to these photo-generated electron-hole pairs. However, the slow photocurrent response (30 s during rise and more than 150 s during decay) is not likely to be due to the slow mobility/separation of electrons/holes. Notably, the photo-induced H_2O_2 decomposition usually takes much longer, as shown in figure S16 and previous studies.[52] Hence, the slow photocurrent response with illumination is probably due to the decomposition of H_2O_2. This would also explain why the slow response (figure 7) is only obvious in the presence of BAN but not in Bi buffer. As a result, the effect of the light on the photocurrent is improved not only improving the MnO_x activity but also by accelerating the H_2O_2 decomposition.

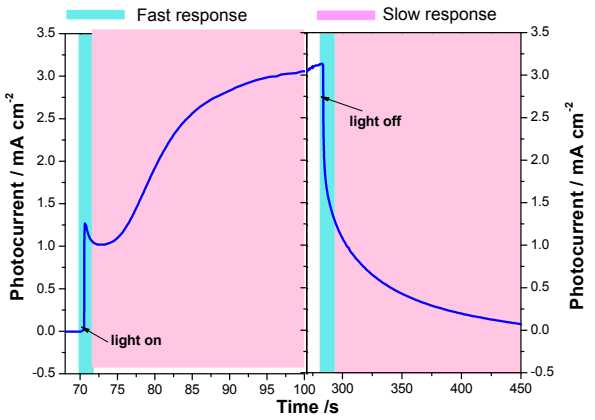

Figure 11. Transient photocurrent of a MnO_x film in Bi+BAN at 1.0 V with light on and light off. The photocurrent is composed of a fast reponse and slow response, marked as blue and pink, respectively.

In addition to the BAN contributing to the high photocurrent, the buffered conditions have a strong influence on the generation of a high photocurrent. This effect of buffering on maintaining a high water oxidation activity is also reported for a cobalt based catalyst.[57] The 1.0 M BAN solution (10 ml) at pH9 contains 1.2 mol% (120 µmol) of free amine, while the 1.0 M BAN at pH10 contains 11.2% free amine (1120 µmol). As the pKa of butyl amine is 10.59 and the range of pKa±1 can be considered as the effective buffer region, the BAN at pH10 can be expected to act as a buffer while the BAN at pH9 has very low buffer capacity. In the un-buffered BAN electrolyte, the accumulation of H^+ on the surface generated via equation 1 *(6.22 µmol over 2hrs)* is small compared with the excess amine in the bulk electrolytes, but it could significantly influence the local proton activity on the surface (for example there is only *1.5 µmol* excess amine in a 0.5 cm thick diffusion layer at the electrode). Thus, a decrease in the local pH could occur on the catalyst surface. As the photo-electrochemical water oxidation is pH dependent (E_0 (V) =1.23 - 0.059 x pH), the decrease in local pH results in a decrease in the effective overpotential. This in turn decreases both the dark and photocurrent as shown in BAN at pH9. On the other hand, in the pH10 BAN electrolyte, which has sufficient proton-accepting capacity, the pH on the surface is more stable than in the un-buffered electrolytes. Thus, the buffered BAN electrolytes (i.e., pH10 BAN and pH9 BAN with Bi) exhibit much higher photocurrents than the un-buffered (pH9) BAN. Notably, experiments examining the contributions of the added borate buffer vs bicarbonate buffer indicated that these function in a similar way in maintaining high photocurrents.

An important aspect of this study is the linear relationship between light intensity and photocurrent that is maintained at intensities as high as 9 suns. This is much higher than the normal illumination conditions (~1 sun).[6, 25, 30-32] It has been reported that the photocurrent typically shows a linear relationship at low light intensities, but becomes proportional to the square root of light intensity for TiO_2,[27] or reaches a saturation in the case of CdS[26] at higher illumination intensities. Fe_2O_3 studies have shown a linear relationship at low photocurrent density (< 1 mA cm^{-2}).[28, 29] In this study, however, the MnO_x film shows no limit in photocurrent, even under strong illumination and reaches a high photocurrent at ~9 suns (~ 4.5 mA cm^{-2} at η = 540 mV, as shown in figure 5a).

Although Fe_2O_3 and $BiVO_4$ are highly photo-active, their intrinsic water oxidation activity is not as good as the OECs, such as Co-Pi,[2] MnO_x[3, 16] and NiO_x.[7] Thus, a second phase serving as an OEC has been incorporated with the Fe_2O_3[49, 58] or $BiVO_4$[25, 31, 59] to enhance their overall photo-electrochemical water oxidation performance. The advantage of MnO_x as the photo-anode is that it is not only photo-active as shown in this paper, but is also a highly active and earth-abundant water oxidation catalyst.[3, 16] Thus, high photo-activity and water oxidation performance could, in principle, be achieved on a single MnO_x material, recalling that the band gap in MnO_x is ~2.0 V. Further improvements, in particular in the photo-voltage generated, might stem from further studies of the photo excitation process in MnO_x, as has been achieved in recent years with Fe_2O_3.[6, 28, 29, 60]

4. Summary and Conclusions

This work has examined the photo-electrochemical performance of MnO_x with respect to the water oxidation reaction. Investigations of the effect of film thickness, substrate, illumination direction and electrolyte on the water oxidation reaction have led to the following findings:

1) Water oxidation performance on MnO_x can be improved by illumination, and the buffered amine ionic liquid electrolytes significantly enhance the photo-electrochemical activity by producing H_2O_2 and O_2 at the same time.

2) The photocurrent generation can in part be attributed to accelerated decomposition of H_2O_2 under light.

3) The highest photocurrent is achieved on MnO_x films with a thickness of 4 µm.

4) The photocurrent is linearly dependent on light intensity.

This study provides an alternative method to improve the photo-activity in water oxidation catalysis. It shows that MnO_x is not only a very good electro-catalyst, but is also a promising photo-anode for water oxidation. Further investigations of the relationship between photo-activity and the crystal structure, morphology, electronic structure, and charge transport behaviour could contribute to yet further improvements in the photo-electrochemical performance of MnO_x.

Acknowledgements

DRM and LS gratefully acknowledge funding from the Australian Research Council (ARC) and ARC Centre of Excellence for

Electromaterials Science (ACES) as well as funding (DRM) from the Australian Laureate Fellowship scheme. FLZ is grateful to Australian Postgraduate Award (APA) and Endeavour International Postgraduate Research Scholarship (IPRS). The authors would like to acknowledge Monash University Centre for Electron Microscopy for providing electron microscopic facilities and F. Huang for helpful discussion.

Notes and references

1 M. Gratzel, Nature 2001, 414, 338.
2 M. W. Kanan, D. G. Nocera, Science 2008, 321, 1072.
3 I. Zaharieva, P. Chernev, M. Risch, K. Klingan, M. Kohlhoff, A. Fischerb, H. Dau, Energy Environ. Sci. 2012, 5, 7081.
4 M. Huynh, D. K. Bediako, D. G. Nocera, J. Am. Chem. Soc. 2014, 136, 6002−6010; M. Busch, E. Ahlberg, I. Panas, J. Phys. Chem. C 2013, 117, 288; P. W. Menezes, A. Indra, P. Littlewood, M. Schwarze, C. Goebel, R. Schomaecker, M. Driess, Chemsuschem 2014, 7, 2202; X. Yang, C. Du, J. Xie, D. Wang. J. Catal. 2013, 304, 86; N. C. Srandwiz, D. J. Comstock, R. L. Grimm, A. C. Nichols-Nielander, J. Elam, N. S. Lewis. J. Phys. Chem. C 2013, 117, 4931.
5 M. W. Kanan, J. Yano, Y. Surendranath, M. Dinca, Y. Yachandra, D. G. Nocera, J. Am. Chem. Soc. 2010, 132, 13692.
6 K. Sivula, F. L. Formal, M. Gratzel, ChemSusChem 2011, 4, 432.
7 M. Dincă, Y. Surendranath, D. G. Nocera, PNAS 2010, 107, 10337.
8 M. M. Najafpour, S. Heidari, E. Amini, K. M. , R. Carpentier, S. I. Allakhverdiev, J. Photochem. Photobiol., B 2014, 133, 124.
9 R. Brimblecombe, A. Koo, G. C. Dismukes, G. F. Swiegers, L. Spiccia, J. Am. Chem. Soc. 2010, 132, 2892.
10 R. K. Hocking, R. Brimblecombe, L. Y. Chang, A. Singh, M. H. Cheah, C. Glover, W. H. Casey, L. Spiccia, Nat Chem 2011, 3, 461.
11 T. Takashima, K. Hashimoto, R. Nakamura, J. Am. Chem. Soc. 2012, 134, 1519.
12 Y. Meng, W. Song, H. Huang, Z. Ren, S.-Y. Chen, S. L. Suib, J. Am. Chem. Soc. 2014, 136, 11452.
13 M. Fekete, R. K. Hocking, S. L.-Y. Chang, C. Italiano, A. F. Patti, F. Arena, L. Spiccia, Energy Environ. Sci. 2013, 6, 2222.
14 K. L. Pickrahn, S. W. Park , Y. Gorlin , H.-B.-R. Lee , T. F. Jaramillo , S. F. Bent, Adv. Energy Mater. 2012, 2, 1269.
15 M. R. Gao, Y. F. Xu, J. Jiang, Y. R. Zheng, S. H. Yu, J. Am. Chem.Soc. 2012, 134, 2930−2933.
16 F. L. Zhou, A. Izgorodin, R. K. Hocking, L. Spiccia, D. R. MacFarlane, Adv. Energy Mater. 2012, 2, 1013.
17 S. Crawford, E. Thimsen, P. Biswas, J. Electrochem. Soc. 2009, 156, H346.
18 A. Izgorodin , E. Izgorodina, D. R. MacFarlane, Energy Environ. Sci. 2012, 5, 9496.
19 C. McDonnell-Worth, D. R. MacFarlane, RSC Adv. 2014, 4, 30551.
20 D. M. Sherman, Geochimica Et Cosmochimica Acta 2005, 69, 3249.
21 C. Sun, Y. Wang, J. Zou, S. C. Smith, Phys. Chem. Chem. Phys. 2011, 13, 11325; S. Pishdadian, A. M. S. Ghaleno, Acta Phys. Pol., A 2013, 123, 741.
22 B. A. Pinaud, Z. B. Chen, D. N. Abram, T. F. Jaramillo, J. Phys. Chem. C 2011, 115, 11830.
23 N. Sakai, Y. Ebina, K. Takada, T. Sasaki, J. Phys. Chem. B 2005, 109, 9651.
24 A. Singh, R. K. Hocking, S. L.-Y. Chang, B. M. George, M. Fehr, K. Lips, A. Schnegg, L. Spiccia, Chem. Mater. 2013, 25, 1098
25 T. W. Kim , K.-S. Choi, Science 2014, 343, 990.
26 R. H. Bube, J. Appl. Phys 1960, 31, 1301.
27 T.-H. Lim, S.-D. Kim, Korean J. Chem. Eng. 2002, 19, 1072.
28 S. R. Pendlebury, A. J. Cowan, M. Barroso, K. Sivula, J. Ye, M. Gratzel, D. R. Klug, J. Tang, J. R. Durrant, Energy Environ. Sci. 2012, 5, 6304; I. Cesar, K. A., J. A. G. Martinez, M. Gratzel, J. Am. Chem. Soc. 2006, 128, 4582.
29 B. D. Chernomordik, H. B. Russell, U. Cvelbar, J. B. Jasinski, V. Kumar, T. Deutsch, M. K. Sunkara, Nanotechnology 2012, 23, 194009.
30 B. Klahr, S. Gimenez, F. Fabregat-Santiago, T. Hamann, J. Bisquert, J. Am. Chem. Soc. 2012, 134, 4294.
31 Y. Liang, J. Messinger, Phys. Chem. Chem. Phys. 2014, 16, 12014.
32 M. Fekete, W. Ludwig, S. Gledhill, J. Chen, A. Patti, L. Spiccia, Eur. J. Inorg. Chem. 2014, 2014, 750.
33 Mathias, Solar Cell Efficiency World Record Set By Sharp - 44.4%,http://cleantechnica.com/2013/06/23/solar-cell-efficiency-world-record-set-by-sharp-44-4/, July, 2013.
34 H. Dotan, K. Sivula, M. Gratzel, A. Rothschild, S. C. Warren, Energy Environ. Sci. 2011, 4, 958.
35 J. Nissfolk, K. Fredin, J. Simiyu, L. Häggman, A. Hagfeldt, G. Boschloo, J. Electroanal. Chem. 2010, 646, 91.
36 B. Yang, P. R. F. Barnes, W. Bertram, V. Luca, J. Mater. Chem. 2007, 17, 2722.
37 Y. C. Ling, G. M. Wang, D. A. Wheeler, J. Z. Zhang, L. Yat, Nano Lett. 2011, 11, 2119.
38 F. L. Zhou, A. Izgorodin, R. K. Hocking, V. Armel, L. Spiccia, D. R. MacFarlane, Chemsuschem 2013, 6, 643.
39 K. L. Pickrahn, S. W. Park, Y. Gorlin, H.-B.-R. Lee, T. F. Jaramillo, S. F. Bent, Advanced Energy Materials 2012, 2, 1269.
40 T. Lindgren, H. Wang, N. Beermann, L. Vayssieres, A. Hagfeldt, S.-E. Lindquist, Sol. Energy Mater. Sol. Cells 2002, 71, 231.
41 S. Bai, C. Wang, M. Deng, M. Gong, Y. Bai, J. Jiang, Y. Xiong, Angew. Chem. Int. Ed. 2014, 53, 12120.
42 H. Hall, J. Am. Chem. Soc. 1957, 79, 5441.
43 J. M. Beale, J. H. Block, Eds., *Wilson and Gisvold's Textbook of Organic Medicinal Pharmaceutical Chemistry- 12th Edition*, Lippincott Williams & Wilkins, Philadelphia, PA, USA 2009.
44 J. Long, H. Chang, Q. Gu, J. Xu, L. Fan, S. Wang, Y. Zhou, W. Wei, L. Huang, X. Wang, P. Liu, W. Huang, Energy Environ. Sci. 2014, 7, 973; S. Dhara, P. Giri, Nanoscale Res. Lett. 2011, 6, 504.
45 F. Fabregat-Santiago, G. Garcia-Belmonte, J. Bisquert, A. Zaban, P. Salvador, *J. Phys. Chem. B* 2002, 106, 334.
46 [46]A. K. Manohar, O. Bretschger, K. H. Nealson, F. Mansfeld, Electrochim. Acta 2008, 53, 3508; A. K. Manohar, O. Bretschger, K. H. Nealson, F. Mansfeld, Bioelectrochemistry 2008, 72, 149.
47 K. D. Kwon, K. Refson, G. Sposito, Physical Review Letters 2008, 100, 146601.
48 S. Banerjee, J. Gopal, P. Muraleedharan, A. K. Tyagi, B. Raj, Curr. Sci. 2006, 90, 1378.
49 J. Y. Kim, G. Magesh, D. H. Youn, J.-W. Jang, J. Kubota, K. Domen, J. S. Lee, Sci. Rep. 2013, 3, 2681.
50 Y. Chiba, A. Islam, Y. Watanabe, R. Komiya, N. Koide, L. Han, Jpn. J. Appl. Phys. 2006, 40, L638.
51 I. Katsounaros, W. B. Schneider, J. C. Meier, U. Benedikt, P. U. Biedermann, A. A. Auer, K. J. J. Mayrhofer, Phys. Chem. Chem. Phys. 2012, 14, 7384; W. Jia , M. Guo , Z. Zheng , T. Yu, E. G. Rodriguez, Y. Wang, Y. Lei, J. Electroanal. Chem. 2009, 625, 27.
52 C. A. Páez , D. Y. Liquet , C. Calberg, S. D. Lambert, I. Willems, A. Germeau, J.-P. Pirard, B. Heinrichs, Catal. Commun. 2011, 15, 132.
53 H. Dau, C. Limberg, T. Reier, M. Risch, S. Roggan, P. Strasser, ChemCatChem 2010, 2, 724.
54 S. P. Mehandru, A. B. Anderson, J. Electrochem. Soc. 1989, 136, 158.
55 J. O. M. Bockris, T. Otagawa, J. Phys. Chem. B 1983, 87,, 2960; J. O. M. Bockris, T. Otagawa, V. Young, J. Electroanal. Chem. 1983, 150, 633.
56 D. Tafalla, P. Salvador, R. M. Benito, J. Electrochem. Soc. 1990, 137, 1810.
57 Y. Surendranath, M. Dinca, D. G. Nocera, J. Am. Chem. Soc. 2009, 131, 2615.
58 D. K. Zhong, M. Cornuz., K. Sivula., M. Grätzel., D. R. Gamelin, Energy Environ. Sci. 2011, 4, 1759.
59 M. Zhou, J. Bao, W. Bi, Y. Zeng, R. Zhu, M. Tao, Y. Xie, Chemsuschem 2012, 5, 1420.
60 J. H. Kennedy, K. W. Frese, J. Electrochem. Soc. 1978, 125, 709; A. Duret, M. Gratzel, J. Phys. Chem. B 2005, 109, 17184.